Control Design of Hard Disk Drive Concentric Self-Servo Track Writing via H_2 and H_∞ Synthesis

Jianbin Nie and Roberto Horowitz

Computer Mechanics Laboratory
Mechanical Engineering
University of California, Berkeley, CA, USA

January 2, 2012

Abstract

This paper considers two novel controller synthesis methodologies using a feedforward control structure for performing concentric self-servo track writing in hard disk drives. In the first methodology, it is assumed that a conventional causal track-following controller has been designed and a non-causal feedforward controller, which utilizes the stored error signal from writing the previous track, is designed using standard H_∞ control synthesis techniques, in order to prevent the track errors from propagating and to achieve good disturbance attenuation. In the second methodology, both the track-following feedback controller and the feedforward controller are simultaneously designed via a mixed H_2/H_∞ control scheme, which involves the solution of a set of linear matrix inequalities and achieves good disturbance attenuation while preventing the propagation of track errors from the previous tracks. Simulation results confirm that the two proposed control synthesis methodologies prevent error propagation from the previously written tracks and significantly improve concentric self-servo track writing performance.

1 Introduction

Modern hard disk drive (HDD) servo systems require that servo patterns, which contain track positioning information, should be embedded on the disk surface at specific locations called servo sectors. Afterwards, the servo patterns on servo sectors are utilized to provide feedback signals for HDD servo systems to position read/write magnetic head. In order to reduce track misregistration [4, 9] and increase track density [19], it is necessary to improve the precision of the servo pattern writing process.

Conventionally, servo patterns are written by costly dedicated servowriting equipment [12] external to disk drives. Self-servo track writing (SSTW) [2, 11] is an alternative method of writing servo patterns using the HDD's own reading and writing heads and servo system, in order to save the process cost and improve the servowriting quality. During SSTW, the timing and radial information are obtained from the previously written track using the read head, while timing and radial positioning servo patterns for the current track are being written using the write head. Consequentially, the external equipment is no longer needed in the servo-pattern writing and thus the servo track writing does not have to be carried out in any clean room environment. There are two most popular SSTW methodologies, spiral-based SSTW [1, 16] and concentric-based SSTW. In this paper, we just focus on the compensation scheme for concentric self-servo track writing. Specifically, the process of the concentric self-servo track writing generally involves the following steps [18]:

1. Write one or more concentric servo sector tracks using conventional servowriting methodologies. These tracks are used as the initial seed tracks, from which reference timing and radial position information is measured to write the next (adjacent) track in a bootstrap manner, and can be pre-written on the disks before the disks are assembled in the HDD.

2. Assume that the read-head to write-head position offset is equal to one track width [5]. Using the read head, collect timing and radial information from the previously written seed track and use this information to generate the position error signals to track follow the seed track, while the write head writes actual servo patterns for the current track.

3. Use the track written in Step 2) as the new seed track and go back to Step 2) until all concentric tracks are written.

However, several challenges arise with the concentric SSTW process such as the fact that radial position errors from the previous track can propagate into the currently written track. This radial positioning error propagation will lead to instability unless it is contained by guaranteeing that the magnitude for the error propagation term is sufficiently attenuated. In order to contain the error propagation, iterative learning control (ILC) and 2-Dimensional H_2 control have been studied in [17] and [8] respectively. In [17], a feedforward based iterative learning control is designed in

the lifted domain assuming zero initial conditions at the beginning of each track servo writing stage and the existence of finite impulse-response (FIR) representations for the servo's sensitivity and complimentary sensitivity functions. However, we note that these assumptions are not strictly true for real HDDs. In [8], a novel 2-Dimensional H_2 control synthesis technique for SSTW is formulated to satisfy a sufficient rather than a necessary condition by making some matrices be block diagonal in order to transfer the optimization to the form of linear matrix inequalities (LMI).

In this paper, we present two novel control synthesis methodologies for performing concentric self-servo track writing in hard disk drives using a feedforward control structure [17, 13]. In the first methodology, a non-causal feedforward controller, which utilizes the stored error signal [13] from writing the previous track, is designed given a pre-defined causal track-following controller. Standard H_∞ control synthesis techniques are used to avoid the propagation of track errors from the previous tracks, while achieving sufficient disturbance attenuation. In the second methodology, an analytic expression for the power spectrum density of track errors is derived and approximated. The approximate expression is subsequently used to formulate the simultaneous design of both a feedback and a feedforward controller, using a mixed H_2/H_∞ control scheme, which ensures the containment of the error propagation and the achievement of good disturbance attenuation and is solved via the solution of a set of LMIs. Neither of these techniques utilizes the simplifying assumptions in [17]. Simulation results based on the HDD benchmark problem developed in [10] show that the controllers synthesized by the proposed schemes outperform the controllers synthesized by the techniques in [17], and offer levels of performance that are comparable to the 2-dimensional H_2 control technique in [8] while having a much simpler control structure.

The paper is organized as follows. Section 2 describes the non-causal feedforward control design by using standard H_∞ control. In Section 3, the analytical expression for the power spectrum density of track errors is derived. Section 4 presents the design of feedback and feedforward controllers by using a mixed H_2/H_∞ control scheme. Simulation results are provided in Section 5. Finally, conclusions are given in Section 6.

2 NON-CAUSAL FEEDFORWARD CONTROL DESIGN VIA H_∞ CONTROL

2.1 Feedforward-control structure based SSTW system

Figure 1 illustrates the block diagram of the concentric self-servo track writing system with a feedforward control structure [13]. The system includes a feedforward controller $F(z)$ and a standard track-following servo loop with the VCM plant $P(z)$ and the feedback controller $C(z)$. In Fig. 1, i and k denote the track index and servo sector index respectively, while $\triangle y_i(k)$, $w_i(k)$, $r_i(k)$ and $n_i(k)$ denote the track error, windage, track runout due to disk vibrations, and measurement noise, respectively, at the position of track i and servo sector k. Similar to [15], d_n, d_w, and d_r are

assumed to be white noises with unit variance. Moreover, since the feedforward controller $F(z)$ utilizes the error signal $e_{i-1}(k)$, which can be stored when writing the previous track, and hence the entire $e_{i-1}(k)$ sequence in (k) is available when writing the current track, a non-causal feedforward controller $F(z)$ is feasible for the control structure in Fig. 1. Here, windage and measurement noise are modeled as white noises with the variance σ_w^2 and σ_n^2 respectively, while the track runout caused by disk vibrations is modeled as a color noise generated by feeding a white noise d_r input to the filter $G_r(z)$.

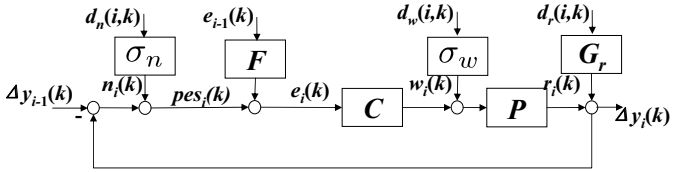

Figure 1: Feedforward control structure based SSTW system

Based on the block diagram in Fig. 1, we can get the following recursive expression for track errors:

$$\begin{aligned} \triangle y_i(k) &= G_1(z)\triangle y_{i-1}(k) + T(z)n_i(k) \\ &\quad + S(z)d_i(k) - S(z)F(z)d_{i-1}(k) \end{aligned} \tag{1}$$

where $T(z) = \frac{P(z)C(z)}{1+P(z)C(z)}$, $S(z) = \frac{1}{1+P(z)C(z)}$, $d_i(k) = P(z)w_i(k) + r_i(k)$, and $G_1(z) = \frac{P(z)C(z)+F(z)}{1+P(z)C(z)}$.

Notice that $G_1(z)$ becomes the key transfer function relating the previous and the current track errors.

2.2 Non-causal feedforward control design

Like the iterative learning control in [17] and [14], a feedback controller $C(z)$ for track following is firstly designed to achieve good disturbance attenuation. Here, $C(z)$ is designed as an optimal H_2 controller. In order to contain the error propagation, the designed controllers must satisfy $\|G_1(e^{j\omega})\|_\infty < 1$. Furthermore, in order to make the error propagation converge as quickly as possible, we want $\|G_1(e^{j\omega})\|_\infty$ to be sufficiently small. From (1), we learn that the current track error is also affected by the disturbances from the previous track. In order not to degrade the disturbance attenuation performance of the track-following controller $C(z)$, the magnitude of the filter $F(z)$ needs to also be sufficiently small. In all, the feedforward control $F(z)$ must be designed to achieve the following target:

$$\begin{cases} \|G_1(z)\|_\infty : \text{sufficiently small and less than 1} \\ \|F(z)\|_\infty : \text{sufficiently small} \end{cases} . \tag{2}$$

As a consequence, we consider the following optimization:

$$\min_{F(z)} \left\| \begin{bmatrix} G_1(z) & w_{t1}F(z) \end{bmatrix} \right\|_\infty \tag{3}$$

where w_{t1} is a weighting value to be tuned to achieve the target in (2). The optimization in (3) is a standard H_∞ control problem, which can be easily solved, as shown later in this section. However, the solution to (3) can only produce a causal compensator $F(z)$ [7]. Obviously, a smaller objective value may be achieved if $F(z)$ is allowed to be non-causal. In order to design a non-causal filter $F(z)$, we consider the following facts:

$$\begin{aligned} \left\| \begin{bmatrix} G_1(z) & w_{t1}F(z) \end{bmatrix} \right\|_\infty &= \left\| \begin{bmatrix} z^{-n_d}G_1(z) & w_{t1}z^{-n_d}F(z) \end{bmatrix} \right\|_\infty \\ &= \left\| \begin{bmatrix} \frac{z^{-n_d}P(z)C(z)+\tilde{F}(z)}{1+P(z)C(z)} & w_{t1}\tilde{F}(z) \end{bmatrix} \right\|_\infty \end{aligned} \tag{4}$$

where $F(z) = z^{n_d}\tilde{F}(z)$ and n_d is a positive integer. Thus, the optimization in (3) can be transformed into the following optimization:

$$\min_{\tilde{F}(z)} \left\| \begin{bmatrix} \frac{z^{-n_d}P(z)C(z)+\tilde{F}(z)}{1+P(z)C(z)} & w_{t1}\tilde{F}(z) \end{bmatrix} \right\|_\infty . \tag{5}$$

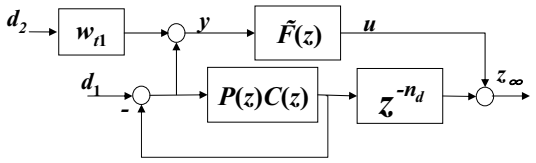

Figure 2: Block diagram for the interpretation of H_∞ norm in (5)

By considering the block diagram in Fig. 2, we have $T_{z_\infty \leftarrow d_\infty} = \begin{bmatrix} \frac{z^{-n_d}P(z)C(z)+\tilde{F}(z)}{1+P(z)C(z)} & w_{t1}\tilde{F}(z) \end{bmatrix}$, where $d_\infty = \begin{bmatrix} d_1 & d_2 \end{bmatrix}^T$. Note that the symbol $T_{A \leftarrow B}$ represents the transfer function from signal B to signal A. Thus, the optimization in (5) can be interpreted as an H_∞ control problem for the linear fractional transformation (LFT) in Fig. 3 to minimize $\|T_{z_\infty \leftarrow d_\infty}\|_\infty$. Here, $G(z)$ is the transfer function matrix from $\begin{bmatrix} d_\infty^T & u \end{bmatrix}^T$ to $\begin{bmatrix} z_\infty^T & y \end{bmatrix}^T$ as shown in Fig. 2.

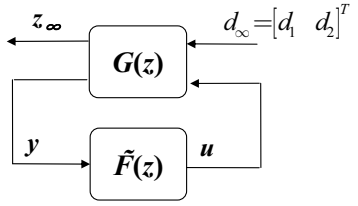

Figure 3: LFT for the H_∞ control design problem

Then, the standard H_∞ control synthesis technique can be applied to the control problem as shown in Fig. 3 to generate the controller $\tilde{F}(z)$. Once a causal $\tilde{F}(z)$ is designed, a non-causal feedforward controller can be constructed from $F(z) = z^{n_d}\tilde{F}(z)$.

3 Track error analysis for the feedforward control based SSTW

3.1 Power spectrum density of track errors

In order to investigate the relationship between the current track error and disturbances from the previously written tracks, we assume that the servo patterns on each track are written after the system reaches its steady state. Then, based on the recursive form of track errors in (1), we have the following complete expression for track errors.

$$\begin{aligned}
\triangle y_i(k) &= G_1^i \triangle y_0(k) + \sum_{l=1}^{i} G_1^{i-l} T n_l(k) + \sum_{l=1}^{i} G_1^{i-l} S d_l(k) \\
&\quad - \sum_{l=1}^{i-1} G_1^{i-1-l} SF d_l(k) \\
&= \sum_{l=1}^{i-1} G_1^{i-1-l} T\left[(T+SF)n_l(k) - S(1-F)d_l(k)\right] \\
&\quad + G_1^i \triangle y_0(k) + T n_i(k) + S d_i(k) \\
&= \sum_{l=1}^{i-1} G_1^{i-1-l} T\left[G_1 n_l(k) - S(1-F)d_l(k)\right] \\
&\quad + G_1^i \triangle y_0(k) + T n_i(k) + S d_i(k)\ . \qquad (6)
\end{aligned}$$

Furthermore, we assume that the seed track error $\triangle y_0$, measurement noises and disturbances are uncorrelated with each other and the track error on the seed track has a power spectrum density $\Phi_{\triangle y_0 \triangle y_0}$. Moreover, measurement noises on different tracks are uncorrelated and have the same variance σ_n^2, while disturbances on different tracks are also uncorrelated and have the same power spectrum density $\Phi_{dd}(e^{j\omega})$. With these assumptions, we can get the following power spectrum density for the track error on track i:

$$\begin{aligned}
\Phi_{\triangle y_i \triangle y_i}(e^{j\omega}) = \sum_{l=1}^{i-1} |G_1|^{2(i-l-1)} |T|^2 \big(|G_1|^2\sigma_n^2 + |S|^2|1-F|^2 \\
\cdot \Phi_{dd}\big) + |G_1|^{2i}\Phi_{\triangle y_0 \triangle y_0} + |T|^2\sigma_n^2 + |S|^2\Phi_{dd}\ . \qquad (7)
\end{aligned}$$

When the track index i is quite large, $\left|G_1(e^{j\omega})\right|^{2i}$ will be closed to zero, since $\left|G_1(e^{j\omega})\right| < 1$. Then, for the large track index i, we have:

$$\begin{aligned}\Phi_{\triangle y_i \triangle y_i}(e^{j\omega}) &= \frac{|T|^2}{1-|G_1|^2}\left[\sigma_n^2 + |\hat{F}|^2\Phi_{dd}(e^{j\omega})\right] \\ &\quad +|S|^2\Phi_{dd}(e^{j\omega})\,. \end{aligned} \tag{8}$$

In order to conveniently synthesize the mixed H_2/H_∞ control, which will be discussed in Section 4, we utilize the parameterization $G_1(z) = 1+\hat{F}(z)$ and $\hat{F}(z) = S(z)\,(F(z)-1)$.

3.2 Discussion

From (8), we note that, in order to reduce track errors, not only a good track-following feedback controller is necessary, but also both $\left|G_1(e^{j\omega})\right|$ and $\left|\hat{F}(e^{j\omega})\right|$ should be sufficiently small. However, $\left|G_1(e^{j\omega})\right|$ and $\left|\hat{F}(e^{j\omega})\right|$ can not be closed to zero at the same time, since $G_1(z) = 1+\hat{F}(z)$. Intuitively, in order to accomplish a good tracking performance, the H_2 norm of the transfer functions from disturbances to track errors must be minimized and simultaneously an appropriately small $\|G_1(z)\|_\infty$ must be guaranteed. This idea turns out to be a mixed H_2/H_∞ control problem, which will be discussed in next section.

4 The design of feedback and feedforward control by using mixed H_2/H_∞ synthesis

4.1 Problem formulation

As discussed in Section 3, (8) educes the idea of a mixed H_2/H_∞ control design in order to achieve a good tracking performance. Let's rewrite (8) as:

$$\begin{aligned}\Phi_{\triangle y_i \triangle y_i}(e^{j\omega}) = |T|^2\left(\frac{\sigma_n^2}{1-|G_1|^2}\right) + |\hat{F}|^2\left(\frac{|T|^2}{1-|G_1|^2}\times\right. \\ \left.\Phi_{dd}(e^{j\omega})\right) + |S|^2\Phi_{dd}(e^{j\omega})\,. \end{aligned} \tag{9}$$

Clearly, (9) demonstrates that the track error can be considered as the output of the system $\bar{G}_2(z) = \begin{bmatrix} T(z) & \hat{F}(z) & S(z)\end{bmatrix}$ with the input of $\begin{bmatrix} \frac{n_i}{\left(1-|G_1|^2\right)^{1/2}} & \frac{T}{\left(1-|G_1|^2\right)^{1/2}}\tilde{d}_i & d_i\end{bmatrix}^T$. Here, $\tilde{d}_i$'s are artificial disturbances, which are uncorrelated with n_i and d_i and have the same power spectrum density as d_i. Notice that the artificial disturbances $\tilde{d}_i$'s are just introduced to represent the second component of the track error power spectrum density in (9).

Since the weighting functions $\frac{1}{\left(1-|G_1|^2\right)^{1/2}}$ and $\frac{T}{\left(1-|G_1|^2\right)^{1/2}}$ for n_i and $\tilde{d}_i$ are not affine in $G_1(z)$ and $T(z)$, the two weighting functions are replaced by two weighting values w_{t2} and w_{t3} respectively, in order to conveniently construct a linear system to represent the transfer function matrix from the input $\begin{bmatrix} n_i & \tilde{d}_i & d_i \end{bmatrix}^T$ to $\triangle y_i$. Such substitution is further validated by the fact that the magnitude frequency responses of both G_1 and T are expected to be flat at low and middle frequencies [17].

By considering the system denoted in Fig. 4 where d_w, d_r, d_n, $\tilde{d}_w$, and $\tilde{d}_r$ are assumed to be uncorrelated white noises, we obtain the following expression for the power spectrum density of z_2:

$$\Phi_{z_2 z_2}(e^{j\omega}) = |T|^2 w_{t2}^2 \sigma_n^2 + |\hat{F}|^2 w_{t3}^2 \Phi_{dd}(e^{j\omega}) + |S|^2 \Phi_{dd}(e^{j\omega}) \,. \tag{10}$$

Obviously, the power spectrum density of z_2 is similar to that of $\triangle y_i$ except the replacement of the weighting functions in (9) with the corresponding weighting values in (10). Thus, with appropriate weighting values w_{t2} and w_{t3}, $\Phi_{\triangle y_i \triangle y_i}(e^{j\omega})$ can be approximated by $\Phi_{z_2 z_2}(e^{j\omega})$. As shown in Fig. 4, let $G_2(z) = \begin{bmatrix} T_{z_2 \leftarrow \begin{bmatrix} d_w & d_r & d_n \end{bmatrix}^T} & w_{t3}\hat{F} * T_{\tilde{d} \leftarrow \begin{bmatrix} \tilde{d}_w & \tilde{d}_r \end{bmatrix}^T} \end{bmatrix}$ denote the transfer function matrix from $\begin{bmatrix} d_w & d_r & d_n & \tilde{d}_w & \tilde{d}_r \end{bmatrix}^T$ to z_2. Therefore, in order to accomplish good track-

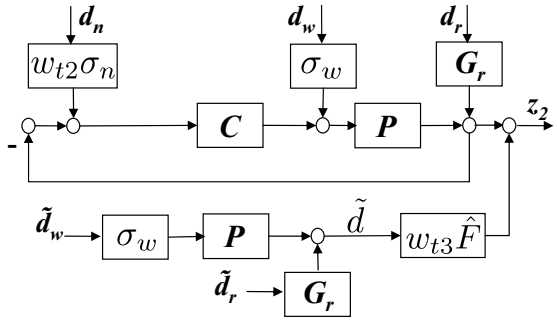

Figure 4: Block diagram for the interpretation of $G_2(z)$

ing error performance, we consider the mixed H_2/H_∞ optimization problem

$$\begin{aligned} \min_{C(z),F(z)} \quad & \|G_2(z)\|_2 \\ \text{s.t.} \quad & \|G_1\|_\infty < \gamma_0 < 1 \end{aligned} \tag{11}$$

to design $C(z)$ and $F(z)$ simultaneously. Here, γ_0 is a given constant to guarantee good convergence for the track error propagation and a good attenuation for the disturbances from the previously written tracks.

4.2 Mixed H_2/H_∞ synthesis via LMIs

A number of techniques [3] have been developed to formulate the mixed H_2/H_∞ control problems such as (11), and the problems are frequently solved as solutions of linear matrix inequalities [15]. However, the mixed H_2/H_∞ optimization in (11) is quite difficult to be solved, because both $G_1(z)$ and $G_2(z)$ not only include the feedback controller $C(z)$ but also the feedforward controller $F(z)$. In order to simplify the synthesis, we utilize the parameterization of $G_1(z) = 1+\hat{F}(z)$. Then, with $\hat{F}(z) = S(z)(F(z)-1)$, the optimization in (11) can be reformulated as:

$$\begin{aligned} \min_{C(z),\hat{F}(z)} \quad & \|G_2(z)\|_2 \\ \text{s.t.} \quad & \|1+\hat{F}(z)\|_\infty < \gamma_0 < 1 \,. \end{aligned} \tag{12}$$

The advantage of the formulation in (12) over the formulation in (11) is that the H_∞ norm constraint only explicitly depends on the parameterization filter $\hat{F}(z)$.

Obviously, $G_2(z)$ can be rewritten as $G_2(z) = \begin{bmatrix} T_{z_2 \leftarrow \begin{bmatrix} d_w & d_r & d_n \end{bmatrix}^T} & 0 & 0 \end{bmatrix} + \hat{F} * \begin{bmatrix} 0 & 0 & 0 & T_{\tilde{d} \leftarrow \begin{bmatrix} \tilde{d}_w & \tilde{d}_r \end{bmatrix}^T} \end{bmatrix}$.

Suppose that we have the following state space realizations:

$$C(z) \sim \left[\begin{array}{c|c} A_c & B_c \\ \hline C_c & D_c \end{array}\right] \tag{13}$$

$$\begin{bmatrix} T_{z_2 \leftarrow \begin{bmatrix} d_w & d_r & d_n \end{bmatrix}^T} & 0 & 0 \end{bmatrix} \sim \left[\begin{array}{c|c} A_{cl2} & B_{cl2} \\ \hline C_{cl2} & D_{cl2} \end{array}\right] \tag{14}$$

$$\begin{bmatrix} 0 & 0 & 0 & T_{\tilde{d} \leftarrow \begin{bmatrix} \tilde{d}_w & \tilde{d}_r \end{bmatrix}^T} \end{bmatrix} \sim \left[\begin{array}{c|c} A_d & B_d \\ \hline C_d & D_d \end{array}\right] \tag{15}$$

$$\hat{F} \sim \left[\begin{array}{c|c} A_{\hat{F}} & B_{\hat{F}} \\ \hline C_{\hat{F}} & D_{\hat{F}} \end{array}\right], G_1 = 1+\hat{F} \sim \left[\begin{array}{c|c} A_{\hat{F}} & B_{\hat{F}} \\ \hline C_{\hat{F}} & 1+D_{\hat{F}} \end{array}\right] \tag{16}$$

$$\hat{F} * \left[\begin{array}{cccc} 0 & 0 & 0 & T \\ & & & {\scriptstyle z_2 \leftarrow}\left[\tilde{d}_w \quad \tilde{d}_r\right]^T \end{array}\right] \sim \left[\begin{array}{c|c} \bar{A}_f & \bar{B}_f \\ \hline \bar{C}_f & \bar{D}_f \end{array}\right]$$

$$= \left[\begin{array}{cc|c} \bar{A}_d & 0 & B_d \\ B_{\hat{F}} C_d & A_{\hat{F}} & B_{\hat{F}} D_d \\ \hline D_{\hat{F}} C_d & C_{\hat{F}} & D_{\hat{F}} D_d \end{array}\right] \tag{17}$$

$$G_2 \sim \left[\begin{array}{c|c} \bar{A}_{cl2} & \bar{B}_{cl2} \\ \hline \bar{C}_{cl2} & \bar{D}_{cl2} \end{array}\right] = \left[\begin{array}{cc|c} \bar{A}_{cl2} & 0 & B_{cl2} \\ 0 & \bar{A}_f & \bar{B}_f \\ \hline C_{cl2} & \bar{C}_f & D_{cl2} + \bar{D}_f \end{array}\right] . \tag{18}$$

Then the optimization in (12) can be synthesized as the following optimization [3]:

$$\min_{A_c, B_c, C_c, D_c, C_{\hat{F}}, D_{\hat{F}}} \operatorname{trace}(W)$$

$$\text{s.t.} \quad \begin{bmatrix} W & \bar{C}_{cl2} & \bar{D}_{cl2} \\ * & X_2 & 0 \\ * & * & I \end{bmatrix} \succ 0 \tag{19}$$

$$\begin{bmatrix} X_2 & X_2 \bar{A}_{cl2} & P_2 \bar{B}_{cl2} \\ * & X_2 & 0 \\ * & * & I \end{bmatrix} \succ 0 \tag{20}$$

$$\begin{bmatrix} X_1 & X_1 A_{\hat{F}} & X_1 B_{\hat{F}} & 0 \\ * & X_1 & 0 & C_{\hat{F}}^T \\ * & * & I & 1 + D_{\hat{F}}^T \\ * & * & * & \gamma_0^2 I \end{bmatrix} \succ 0 \tag{21}$$

where the symbol "$*$" denotes the transpose of the corresponding element at its transposed position. Since both X_1 and X_2 are coupled with $A_{\hat{F}}$ and $B_{\hat{F}}$ in (21) and (20) respectively, the filter $\hat{F}(z)$ is chosen as an FIR filter, which means that $A_{\hat{F}}$ and $B_{\hat{F}}$ are known and thus (21) becomes an LMI. Moreover, in order to recover the convexity of (19) and (20) by an appropriate nonlinear transformation [6], the matrix X_2 is chosen as a block diagonal matrix, i.e., $X_2 = \operatorname{diag}\left\{X_{22}, X_{ff}\right\}$. As a result, the optimization involving (19), (20) and (21) is a convex optimization, which can be easily solved. After synthesizing $\hat{F}(z)$, we can reconstruct the feedforward control by

$$F(z) = 1 + S^{-1}(z)\hat{F}(z) = 1 + (1 + P(z)C(z))\hat{F}(z) .$$

5 Simulation Study

In order to evaluate the concentric SSTW design methodologies presented in this paper, they will be tested through a simulation study that utilizes the benchmark model developed by the IEEJapan technical committee on Nano-Scale Servo (NSS) system [10]. This model was also utilized to test the concentric SSTW design scheme presented in [17]. This benchmark model was originally developed to test track-following servos and must be modified to test servo systems for self-servo track writing control. For the simulated drive, the servo sector number N is equal to 220 and the disk rotation speed is 7200 RPM. Thus, the sampling frequency for this drive is $f_s = 220 * 7200/60 = 26400$ Hz.

5.1 Weighting value determination

Before using the presented two control synthesis methodologies, we have to determine the corresponding weighting values w_{t1}, w_{t2}, and w_{t3}. For the technique presented in Section 2, since the track error propagation term G_1 may result in instability (if $\|G_1(z)\|_\infty > 1$), it is reasonable to choose a relatively small w_{t1}. Intuitively, the selection of $w_{t1} < 1$ is desirable to emphasize G_1. For the technique presented in Section 4, γ_0 must be less than 1 and is required to be closed to 1 so that the obtained H_2 norm cost for track errors in (11) is not too conservative according to the H_∞ norm constraint. In addition, w_{t2} and w_{t3} are utilized to approximate $\frac{1}{\left(1-|G_1|^2\right)^{1/2}}$ and $\frac{T}{\left(1-|G_1|^2\right)^{1/2}}$ respectively. As mentioned in Section 4, the magnitude of T and G_1 are flat at the low and middle frequencies and thus it is desirable to determine w_{t2} and w_{t3} using the DC gains of T and G_1. It is well known that in order to attenuate low-frequency disturbances, $T = \frac{PC}{1+PC}$ is usually designed to have a unit DC gain. Thus, w_{t2} and w_{t3} can be roughly selected by

$$w_{t2} = w_{t3} = \frac{1}{\left(1 - (\text{Expected DC Gain of } G_1)^2\right)^{1/2}}.$$

5.2 Control design results

An optimal H_2 track following compensator $C(z)$ was first synthesized and then a non-causal feedforward compensator $F(z)$ was designed using the H_∞ control design methodology presented in Section 2, with the weighting value $w_{t1} = 0.16$ and $n_d = 7$. The designed control system achieves $\|G_1(z)\|_\infty = 0.9781 < 1$ and $\|F(z)\|_\infty = 1.3633$. The corresponding frequency response plots for the designed $F(z)$, $\frac{P(z)C(z)+F(z)}{1+P(z)C(z)}$, $\frac{1}{1+P(z)C(z)}$, and $\frac{F(z)}{1+P(z)C(z)}$ are shown in Fig. 5.

Subsequently, a feedforward compensator $F(z)$ constructed from the FIR filter $\hat{F}(z)$ and a feedback compensator $C(z)$ were simultaneously designed using the mixed H_2/H_∞ control synthesis methodology in Section 4. The designed control system achieves $\|G_1(z)\|_\infty = 0.9737$ with the tuning parameters $w_{t2} = 4$, $w_{t3} = 4$ and $\gamma_0 = 0.98$. The frequency

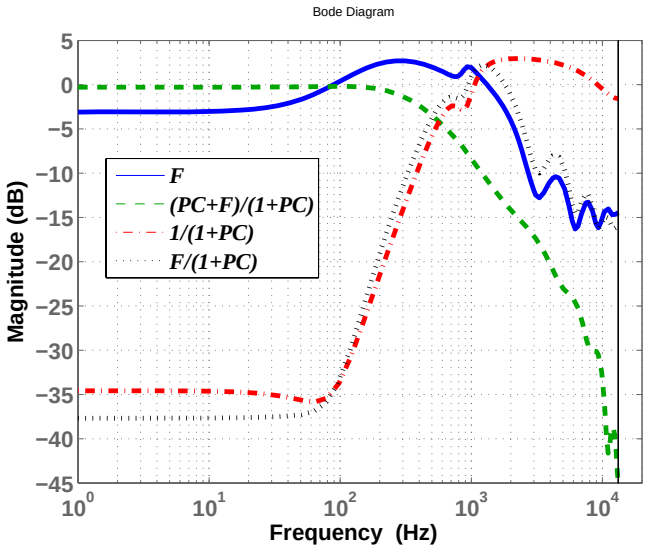

Figure 5: Frequency responses for the non-causal feedforward control design via H_∞ in Section 2

response plots for the resulting controllers are shown in Fig. 6.

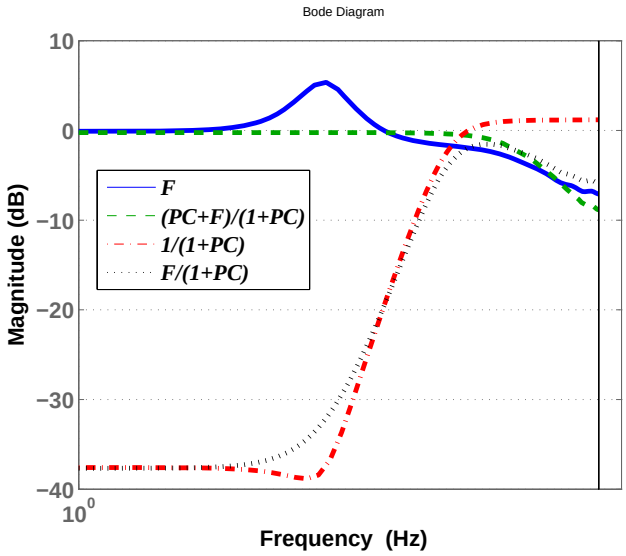

Figure 6: Frequency responses for the feedback and feedforward control designs using the mixed H_2/H_∞ synthesis methodology in Section 4.

5.3 Time-domain simulation results

For the benchmark problem in [10], the modeled sensor noise has a sigma value of 1.5% of track pitch; that of the track runout due to disk vibrations is 1.7% of track pitch; the contribution of the windage at PES has a sigma value of 12.2% track width. The track error for the seed track is assumed to be a sigma value of 14% track width. In the simulation, a total of 5000 servo tracks data was collected. In order to interpret the simulated results better, we also

provide the time-domain simulation results for the 2-Dimensional H_2 SSTW synthesis technique presented in [8]. The sigma values of the first 5000 self-servo written tracks for the proposed two methods in this paper and for the 2-D H_2 system are depicted in Fig. 7. Obviously, the track error propagation is well contained for all the three design methodologies.

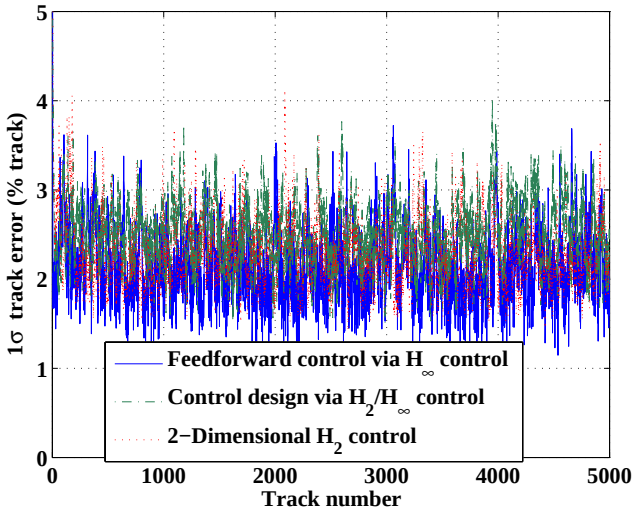

Figure 7: Time domain simulation results for track errors. Since the performance of the control design via H_2/H_∞ is closed to that of 2-D H_2 control, the green dashed line is almost covered by the red dotted line.

Meanwhile, by considering the relatively large variance of the seed track, we are also interested in checking how fast the transition response caused by the seed track can converge. The zoomed in figure for the transition response is illustrated in Fig. 8. The results demonstrate that the effect of the bad seed track on the subsequently written tracks by the proposed controllers disappears very quickly. Specifically, the simulation results show that the transition responses have disappeared after about 15 tracks.

We now consider another common performance index called AC squeeze in order to quantify the quality of written tracks. The AC squeeze for track i is defined as:

$$\text{ACsqueeze}_i = \min_{k\in[0,N-1]} \{1 + \triangle y_i(k) - \triangle y_{i-1}(k)\} \tag{22}$$

where track errors $\triangle y_i(k)$ and $\triangle y_{i-1}(k)$ are normalized by the track width. When the AC squeeze is too small, two adjacent tracks with narrow track spacing may interfere with each other and cause data corruption. The ideal value of AC squeeze is 1 track width, which means the adjacent tracks are perfectly parallel to each other. The AC squeeze values for the simulated self-servo written tracks are shown in Fig. 9. Moreover, the resulting average values of $\sigma(\triangle y_{i-1}(k))$ and ACsqueeze_i are presented in Table 1. Note that the non-causal feedforward control design through standard H_∞ control achieves the best performance for track errors, while the feedback and feedforward control designs

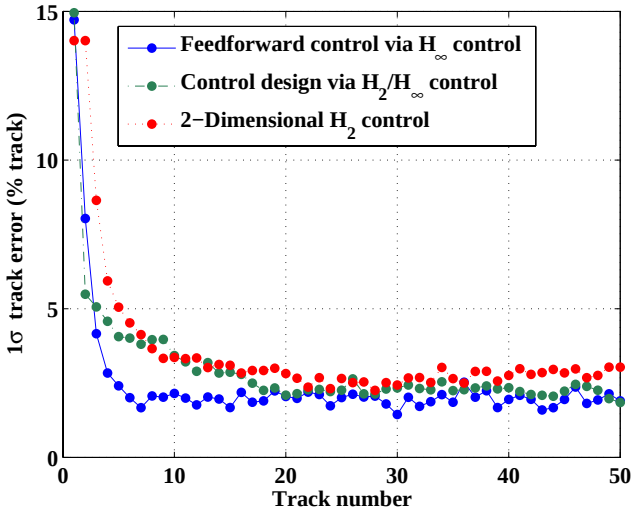

Figure 8: Zoomed in Fig. 7 to check the transition response caused by the seed track.

by using the mixed H_2/H_∞ control accomplish the best AC squeeze.

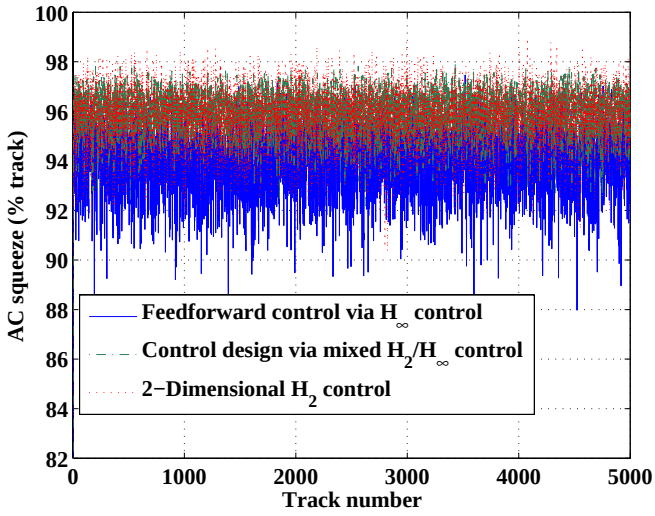

Figure 9: Time domain simulation results for AC Squeeze. Since the performance of the control design via H_2/H_∞ is closed to that of 2-D H_2 control, the green dashed line is almost covered by the red dotted line.

In order to provide the better evaluation for our proposed control synthesis techniques, the simulation results reported in [17] by using the iterative learning control in lifted domain are also listed in Table 1. Obviously, the two proposed control design methodologies are able to improve both track errors and AC squeeze compared to the ILC technique. Meanwhile, the two proposed control design techniques offer the comparable performances to the 2-Dimensional H_2 control technique in [8] while having a much simpler control structure.

Table 1: Simulation Results

	Non-causal feedforward control using H_∞ control	Control designs using mixed H_2/H_∞ control	2-D H_2 control	ILC in lifted domain [21]
Average of 1σ track error (% track)	2.11	2.50	2.27	2.88
Average of AC squeeze (% track)	94.0	96.0	95.8	88

6 Conclusion

This paper discussed two novel controller synthesis methodologies for performing concentric self-servo track writing in hard disk drives using a feedforward control structure. In the first methodology, it is assumed that a conventional causal track-following controller has been designed and then a non-causal feedforward controller, which utilizes the stored error signal from writing the previous track, is designed based on standard H_∞ control synthesis techniques. The designed controllers were used to prevent the track errors from previous tracks from propagating and to achieve good disturbance attenuation. In the second methodology, an analytic expression for the power spectrum density of track errors was approximately derived. The expression was subsequently used to formulate the simultaneous design of both feedback and feedforward controllers, using a mixed H_2/H_∞ control scheme, which ensures the containment of the error propagation and the achievement of good disturbance attenuation and was solved via the solution of a set of LMIs. Neither of these techniques utilizes the simplifying assumptions in [17]. Simulation results using the HDD benchmark problem developed in [10] showed that the controllers synthesized using the proposed schemes outperform the controllers synthesized by the techniques in [17], and offer levels of performances that are comparable with the 2-dimensional H_2 control technique in [8] while having a simpler structure. Moreover, the track error propagation converges after about 15 tracks despite the seed track having a large track error.

Acknowledgment

The authors thank Western Digital Technologies for the motivation of this study. This work was performed with funding support from UC Berkeley Computer Mechanics Laboratory (CML).

References

[1] D. Brunnett, Y. Sun, and L. Guo, "Method and apparatus for performing a self-servo write operation in a disk drive using spiral servo information," U.S. Patent 7230789B1, Jun., 2007.

[2] T. Chainer, M. D. Schultz, B. C. Webb, and E. D. Yarmchuk, "Self servowriting system with dynamic error propagation reduction," U.S. Patent 5793554, Aug. 11, 1998.

[3] X. Chen and K. Zhou, "Multiobjective H_2/H_∞ Control Design", *SIAM J. Control Optim.*, vol. 40, No. 2, pp. 628-660, 2001.

[4] R. Conway and R. Horowitz, "Robust track-following controller design in hard disk drives based on parameter dependent lyapunov functions," *IEEE Trans. Magnetics*, vol. 46, no. 4, pp. 1060-1068, 2010.

[5] D. Cribbs, M. Ellenberger, and J. Hassler, "self-servo writing disk drive and method," U.S. Patent 5448429, 1995.

[6] M. C. De Oliveira, J. C. Geromel, and J. Bernussou, "Extended H_2/H_∞ norm characterization and controller parametrizations for discrete-time systems," *Int. J. Control*, vol. 75, No. 9, pp. 666-679, 2002.

[7] J. C. Doyle, K. Glover, P. Khargonekar, and B. Francis, "State-space solutions to standard H_2 and H_∞ control problems," *IEEE Trans. on Automatic Control*, vol. 34, no. 8, pp. 831-847, 1989.

[8] C. Du, L. Xie, J. N. Teoh, and G. Guo, "H_2 Control for Head Positioning in Axial and Radial Dimensions for Self-Servo Track Writing," *IEEE Trans. on Control Systems Technology*, vol. 16, no. 1, pp. 177-181, 2008.

[9] S. Felix, J. Nie, and R. Horowitz, "Enhanced vibration suppression in hard disk drives using instrumented suspensions," *IEEE Trans. Magnetics*, vol. 45, no. 11, pp. 5188-5122, 2010.

[10] IEEJapan technical committee on Nano-Scale Servo (NSS) system. NSS homepage, 2006. URL http://mizugaki.iis.u-tokyo.ac.jp/nss/.

[11] H.J. Kang, C.W. Lee, C.C. Chung, and H.S. Lee, "Control design for self-servo track writing using a state-space disturbance observer," *IEEE Trans. Magnetics*, vol. 45, no. 11, pp. 5148-5151, 2009.

[12] A. A. Mamun, G. Guo, and C. Bi, *Hard disk drive: mechatronics and control*, Boca Raton, FL: CRC Press, 2007.

[13] H. N. Melkote, R. McNab, B. Cloke, and V. Agarwal, "A study of radial error propagation and self-servowriting in disk drives," *Proceedings of 2002 American Control Conference*, pp. 1372-1377, 2002.

[14] H. Melkote and R. J. McNab, "Modeling and control for self-servowriting in hard disk drives: A repetitive process approach," *Proceedings of the 2006 American Control Conference*, pp. 2005-2010, 2006.

[15] J. Nie and R. Horowitz, "Design and Implementation of Dual-Stage Track-Following Control for Hard Disk Drives," *Proceedings of the Dynamic Systems and Control Conference*, Hollywood, California, 2009.

[16] J. Nie, E. Sheh, and R. Horowitz, "Optimal H_∞ Control for Hard Disk Drives with An Irregular Sampling Rate," *To appear in Proceedings of American Control Conference*, San Francisco, California, 2011.

[17] S. Wu and M. Tomizuka, "An Iterative Learning Control Design for Self-Servowriting in Hard Disk Drives," *Proceedings of the 17th World Congress*, the IFAC, Seoul, Korea, 2008.

[18] H. Ye, V. Sng, C. Du, J. Zhang, and G. Guo, "Radial error propagation issues in self servo track writing technology," *IEEE Trans. On Magnetics*, vol. 38, no. 5, pp. 2180-2182, 2002.

[19] Z. Yuan, B. Liu, T. Zhou, C. Goh, C. Ong, C. Cheong, and L. Wang, "Perspetives of magnetic recording system at 10 Tb/in^2," *IEEE Trans. Magnetics*, vol. 45, no. 11, pp. 5038-5043, 2009.